IEEE Access
Multidisciplinary ⋮ Rapid Review ⋮ Open Access Journal

Received February 11, 2020, accepted February 25, 2020, date of publication March 6, 2020, date of current version March 17, 2020.

Digital Object Identifier 10.1109/ACCESS.2020.2979156

On Design of Protograph LDPC Codes for Large-Scale MIMO Systems

HIEU D. VU[1], THUY V. NGUYEN[1], DIEP N. NGUYEN[2], AND HIEU T. NGUYEN[3]

[1]Faculty of Information Technology, Posts and Telecommunications Institute of Technology, Hanoi 10000, Vietnam
[2]School of Electrical and Data Engineering, University of Technology Sydney, Ultimo, NSW 2007, Australia
[3]Department of Science and Industry Systems, Faculty of Technology, Natural Sciences and Maritime Sciences, University of South-Eastern Norway, 3603 Kongsberg, Norway

Corresponding author: Hieu T. Nguyen (hieu.nguyen@usn.no)

This work was supported by the Vietnam National Foundation for Science and Technology Development (NAFOSTED) under Grant 102.04-2016.23.

ABSTRACT Protograph low-density parity-check (LDPC) codes and large-scale multi-input multi-output (LS-MIMO) systems have achieved great interest with various practical applications. However, how to effectively evaluate and design protograph LDPC codes for LS-MIMO systems remains a challenging yet critical problem, especially for low-latency applications. To solve that design challenge, the protograph extrinsic information transfer chart (PEXIT) algorithm for LS-MIMO systems, so-called LS-MIMO-PEXIT algorithm, is first derived based on the mutual information functions of messages that are passed on the joint MIMO detection and LDPC decoding graph. The proposed LS-MIMO-PEXIT algorithm plays a vital role in the optimization process of designing new protograph LDPC codes, tailored for LS-MIMO communications systems. Experiment results demonstrate that the analytical results based on the LS-MIMO-PEXIT algorithm are in good agreement with the simulation results under various input constraints, including the coding rate, the number of decoding iterations, and the LS-MIMO configuration. On top of that, the new protograph LDPC codes designed using our LS-MIMO-PEXIT algorithm achieve a coding gain from 0.2 dB at a low coding rate to 0.4 dB at a high coding rate in comparison with the state-of-the-art protograph codes in the literature. Additionally, we incorporate the practical design experience and the theoretical analysis of mutual functions into a two-step procedure to search for protograph LDPC codes that do not have error-floor behavior at frame error rate (FER) or bit error rate (BER) as low as 10^{-5} or 10^{-7}, respectively. Together with the coding gain, the error-floor-free feature of the proposed protograph LDPC codes is vitally important for future wireless networks where the ultra-reliability is one of the critical requirements.

INDEX TERMS Large-scale multiple-input multiple-output (LS-MIMO), protograph low-density parity-check (LDPC) codes, channel coding, protograph extrinsic information transfer chart, iterative decoding threshold, low latency.

I. INTRODUCTION

A. MOTIVATION

Thanks to their powerful error-correcting capability and low complexity encoder/decoder structures, protograph LDPC codes have attracted paramount research interest as well as practical applications [1]–[4]. Both LDPC codes and LS-MIMO scheme are two of the core technologies for future wireless networks (6G) [5], [6].

The associate editor coordinating the review of this manuscript and approving it for publication was Oussama Habachi.

However, how to effectively evaluate and design protograph LDPC codes for multi-input multi-output (MIMO) systems with a large number of antennas (referred to as large-scale MIMO or LS-MIMO) remains a challenging yet critical problem. The reason is due to the massive number of antennas that are involved in the detection process and the absence of a systematic tool to iteratively evaluate and optimize the performance of the protograph LDPC codes over LS-MIMO channels to find the optimal proto-matrix of the underlying protograph.

Concerning the latter, we observe that the performance of off-the-shelf protograph LDPC codes designed for AWGN

channels is not fully harvested by the LS-MIMO system, especially for low-delay applications where the number of decoding iterations is limited. As an example, consider the AR4JA [7] and the NND codes [8] that were optimized with a large number of decoding iterations for AWGN channels. Those two codes have the gaps of 0.20 dB and 0.45 dB to the capacity limit, respectively. However, when employing these two codes for the 10 × 10 MIMO configuration and with a given constraint on the number of decoding iterations (e.g., 50 iterations which is a typical value in practical systems [9]), we observed that high-iteration optimized AWGN codes were outperformed by low-iteration optimized AWGN codes - Uchiwaka Code [10] and ATC Code [11].

Moreover, an additional coding gain of 0.2 dB can be harvested, as shown in Fig. 1, if we incorporate features of the joint LS-MIMO detection and protograph LDPC decoding into the design of a new protograph LDPC code for LS-MIMO channels. Additionally, as shown later in this article, existing approaches in the literature, e.g., the conventional protograph extrinsic transfer chart (PEXIT) algorithm [12], its variant for space-time code systems [13], [14] are unable to assess protograph LDPC code's performance and to design new protograph LDPC codes for LS-MIMO channels.

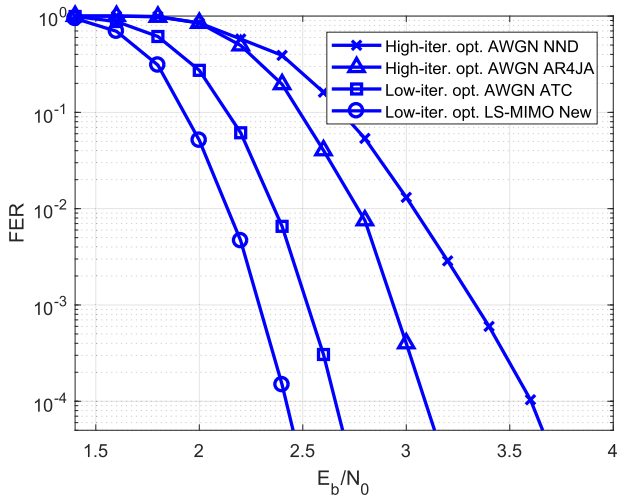

FIGURE 1. FER performance of off-the-shelf and a new protograph LDPC codes: coding rate $R = 1/2$, information blocklength 2400 bits, 50 iterations, 10 × 10 MIMO.

B. RELATED WORKS

The LS-MIMO systems where the hundreds of antennas are used in order to improve the performance of wireless communications have been active research topics recently [15]. Once the number of antennas is in order of from tens to hundreds, the LS-MIMO signal detection is one of the technical challenges. The challenge comes from the fact that many conventional MIMO detection techniques, for example, zero-forcing, maximum likelihood detection, and sphere decoding techniques, have the complexity which is proportional to the cubed number of antennas [16] or even exponential order of the number of antennas. The LS-MIMO belief propagation detection algorithm proposed by Fukada *et al.* [16] can be considered a promising approach to reduce the complexity of the LS-MIMO detector to the second-order calculations. Recently, the LS-MIMO signal detection based on the belief propagation technique has been extended to LS-MIMO systems with the low-resolution ADCs by Vu *et al.* [17].

Deep-learning techniques have newly been used to deal with the complexity of the LS-MIMO signal detection (see [18] and references therein). By unfolding the iterations of a projected gradient descent algorithm, the structure of DetNet is built where each layer is equivalent to an iteration of the conventional iterative detection. The deep-learning approach can achieve state-of-the-art performance while maintaining low computational requirements. In [19], Takabe *et al.* attempted to use the deep-aided iterative detection algorithm for massive MIMO systems where the number of transmit antennas is larger than the number of receive antennas. The complexity of this new detector is proportional to the product of transmit and receive antennas. Notably, the number of trainable parameters is independent of the number of antennas - this makes the training process quick and stable. By letting the deep neural network (DNN) learn the radius of the decoding hypersphere of the conventional sphere decoding [20], a new sphere decoding algorithm is proposed to reduce the complexity of the LS-MIMO signal detector significantly [21]. Observing from the fact that deepening the network does not gain a meaningful performance beyond a certain number of layers, a parallel deep-learning network was developed to obtain diversity effects. As a result, the performance of the LS-MIMO detector under time-varying MIMO channels is improved [22].

As far as the design of powerful error-correcting codes is concerned, low-density parity-check (LDPC) codes [23] have been an active research topic in the coding community due to their excellent error-correcting capability. In most practical applications, quasi-cyclic (QC) structured LDPCs [24], whose parity check matrices are produced by using circulant structures, are broadly adopted because of their linear encoding and decoding complexity. One type of the QC-LDPC code is the protograph LDPC code [7] whose parity-check matrix is built from a small graph, so-called protograph. Protograph LDPC codes have demonstrated remarkable iterative decoding thresholds with low encoder complexity as well as fast decoding [7], [25]. Because of their unique simplicities and representation, protograph LDPC codes have received considerable recognition and have been proposed as error-correcting codes for current and future wireless communications systems [1], [5], [6].

When it comes to the development of protograph LDPC code families, Divsalar *et al.* was the first group that designed many excellent protograph LDPC codes [7]. Those codes have typical minimum distances that grow linearly with the blocklength, and their iterative decoding thresholds approach the Shannon limits on binary-input additive white Gaussian noise (AWGN) channels. Nguyen *et al.* [8] extended the

ideas of Divsalar *et al.* [7] to develop a more generic code structure that resulted in better protograph LDPC codes. Protograph LDPC codes designed in [7], [8] have powerful error-correcting capabilities under a large number of decoding iterations. In contrast, those codes may not be suitable and optimal for many practical applications where complexity and processing delay are strictly limited (i.e., the number of decoding iterations is small). Recently, many research works attempted to design protograph LDPC codes for a small number of decoding iterations [10], [11], [26]. The experiment results proved that the low-iteration optimized codes outperform the high-iteration optimized codes such as NND code [8].

In point-to-point fading channels, Fang *et al.* [27] investigated the protograph LDPC codes for bandwidth-efficient communication systems where the joint protograph LDPC decoding and bit-interleaved coded modulation with iterative demapping and decoding is used. Notably, the proposed communication system approaches the outage-limit performance over block-fading channels by taking the fading-block length into the design of the modulation strategy and incorporating the unequal error protection feature into the bit-to-symbol mapping scheme. Furthermore, for the sake of review's completeness, it should be mentioned that protograph LDPC codes are also attractive in the field of data storage (see [28] and references therein) and the joint design of source and channel coding on a double protograph is an alternative approach to avoid the breakdown of the end-to-end communication link [29].

Designing the LDPC codes for wireless fading channels where multiple antennas are utilized at both sides of a communication link was first performed by ten Brink *et al.* [30]. In this work, the MIMO detector performs APP detection by considering all possible hypotheses of the transmitted MIMO symbol. Later, this design approach was applied to design irregular LDPC codes for LS-MIMO channels [14]. Even though the latter work introduced the design framework for LS-MIMO channels, the core element of the design is based on the standard PEXIT algorithm, which is not applicable to design protograph LDPC codes [12]. Recently, Nguyen *et al.* [31], introduced a PEXIT algorithm for LS-MIMO channels with low-resolution analog-to-digital converters (ADCs). This work was the first research attempt to handle the dynamic interaction of extrinsic information between the MIMO signal detection and the protograph LDPC decoding. The research results reported the performance of the LS-MIMO systems under different resolution levels of the ADCs. To our best knowledge, the research work on the framework to design protograph LDPC codes for LS-MIMO channels remains unsolved, especially for low-latency applications. For this reason, in this paper, we will develop a framework to design new protograph LDPC codes from scratch. The novel idea is to rebuild the PEXIT algorithm for LS-MIMO channels, where the dynamic interaction of extrinsic information between the LS-MIMO signal detector and the protograph LDPC decoder is taken into account. Ultimately, the new protograph LDPC codes outperform state-of-the-art protograph LDPC codes.

C. CONTRIBUTIONS

Given the above, this work aims to provide a framework to design new protograph LDPC codes for LS-MIMO systems from scratch, targeting emerging low-latency applications in 5G and beyond. Specifically, leveraging the factor graph-based detection [16] and the PEXIT algorithm [12]–[14], we use the novel idea of joint detection and decoding Tanner graph first to derive the LS-MIMO-PEXIT algorithm. Then, we incorporate the new LS-MIMO-PEXIT algorithm into our design framework as a central element for establishing a mathematical optimization problem. The proposed new code design framework takes into account three different design dimensions: 1) the propagation characteristics of LS-MIMO channels; 2) the protomatrix structure of a protograph LDPC code; 3) the maximum number of decoding iterations to further optimize the protograph LDPC codes for LS-MIMO channels in the low-iteration regime. Our main contributions are summarized as follows:

- Derive a novel LS-MIMO-PEXIT algorithm based on the double-layer graph for LS-MIMO channels where the joint belief propagation MIMO detection with parallel interference cancellation and the protograph LDPC decoding architecture are used.
- The proposed LS-MIMO PEXIT algorithm allows us to systematically evaluate the performance of off-the-shelf protograph LDPC codes under different input parameters, including the coding rate, the maximum number of decoding iterations, and the LS-MIMO configuration.
- The LS-MIMO PEXIT algorithm facilitates the design of new protograph LDPC codes for specific LS-MIMO systems with a target number of decoding iterations.
- As an example, we design novel protograph LDPC codes for LS-MIMO channels at various coding rates (1/2, 2/3, 3/4) that outperform the state-of-the-art codes (e.g., [9], [10], [13]), with coding gains varying from 0.2 dB to 0.4 dB at FER = 10^{-4}.
- We incorporate the practical design experience and the theoretical analysis of mutual functions into a two-step procedure to search for protograph LDPC codes that do not have error-floor behavior at FER or BER as low as 10^{-5} or 10^{-7}, respectively. Together with the coding gains mentioned above, the error-floor-free feature of the proposed protograph LDPC codes is vitally important for future wireless networks where the ultra-reliability is one of the critical requirements.

D. OUTLINE

The rest of this paper is organized as follows: Section II presents the LS-MIMO channel model and the calculation of the log-likelihood ratio (LLR) messages for each pair of an observation node and a symbol node on the joint LS-MIMO signal detection and the protograph LDPC decoding graph. In Section III, we propose a new version of the PEXIT

algorithm, which is then employed as a core element in the design framework of protograph LDPC codes for LS-MIMO channels. In Section IV, we establish the optimization problem and impose the constraints in order to obtain a feasible search space for the optimization problem. Section V presents protomatrices of the new protograph LDPC codes, which are optimized for the 10×10 MIMO configuration, for different coding rates, and different constraints on the maximum number of decoding iterations. In this section, we also outline a two-step procedure to search for new protograph LDPC codes that do not have the error-floor behavior at the FER level as low as 10^{-5}. Additionally, extensive simulation results are included to verify the analytical performance of the new protograph LDPC codes. Section VI concludes the paper.

II. SYSTEM MODEL

Consider an LS-MIMO channel with M transmit and N receive antennas. A block of K information bits is first encoded by a protograph LDPC encoder that produces a codeword with a length of L coded bits. The coded bit sequence is then modulated by the binary phase-shift keying (BPSK) modulator with the alphabet in $\{+1, -1\}$. In one channel use, M modulated symbols can be transmitted over M transmit antennas using the spatial multiplexing scheme. Consequently, it requires $L_c = \lceil L/M \rceil$ channel uses to transfer all L coded bits. The received signal model is given by

$$\mathbf{y} = \mathbf{H}\mathbf{x} + \mathbf{w}, \tag{1}$$

where $\mathbf{x} = [x[1], x[2], \cdots, x[M]]^T$ is the vector of transmitted symbol whose elements belong to the BPSK modulation alphabet. $\mathbf{H} \in \mathbb{C}^{N \times M}$ is channel matrix whose entries $h[n, m]$ are i.i.d complex Gaussian with zero mean and unit variance $\mathcal{CN}(0, 1)$. For the analysis in the sequel, we assume that the perfect channel state information (CSI) is available at the receiver only. $\mathbf{w} = [w[1], w[2], \cdots, w[N]]^T \in C^{N \times 1}$ denotes the additive noise vector whose elements are i.i.d complex Gaussian random variables with zero mean and variance of N_0, i.e., $\sim \mathcal{CN}(0, N_0)$. $\mathbf{y} = [y[1], y[2], \cdots, y[N]]^T \in \mathbb{C}^{N \times 1}$ is the vector of the received signal at the N receive antennas.

The observation $y[n]$ at the n^{th} receive antenna, which is also referred to as the n^{th} observation node in the Tanner graph, can be written as

$$y[n] = h[n, m]x[m] + \sum_{k=1, k \neq m}^{M} h[n, k]x[k] + w[n]. \tag{2}$$

In the above, the interference component with respect to the transmitted symbol $x[m]$, $\sum_{k=1,k\neq m}^{M} h[n, k]x[k]$, is eliminated by using the parallel interference cancellation technique [16]:

$$\hat{y}[n, m] = y[n] - \sum_{k=1, k \neq m}^{M} h[n, k]\hat{x}[n, k], \tag{3}$$

where $\hat{y}[n, m]$ is the observation of the transmitted symbol $x[m]$ at the n^{th} receive antenna after the interference cancellation. $\hat{x}[n, m]$ is the soft symbol of $x[m]$ at the n^{th} receive antenna.

For the BPSK modulation scheme, the soft symbol $\hat{x}[n, m]$, which is again an estimated version of transmitted symbol $x[m]$ at the n^{th} receive antenna, is obtained using the *tanh*-function as given below:

$$\hat{x}[n, m] = \tanh\left(\frac{\beta[m, n]}{2}\right), \tag{4}$$

where $\beta[m, n]$ is the the extrinsic log-likelihood ratio (LLR) passed from the m^{th} variable node to the n^{th} observation node. It is possible to extend the proposed design to more general complex-valued modulations. For example, we can convert the complex-valued model of the QPSK modulation scheme to the equivalent real-value model of the BPSK modulation scheme. Then we use the formula (4) directly. For the higher-order modulation schemes such as 8-PSK constellation or 16-QAM constellation, the soft symbol estimation is more complicated, and we will investigate this issue in a separate work.

Since the joint LS-MIMO signal detection and protograph LDPC decoding architecture is used, the messages $\beta[m, n]$ in (4) comprise the extrinsic information from both observation nodes of the LS-MIMO detection graph and check nodes of the protograph LDPC decoding graph. In the following section, when a new PEXIT algorithm is derived for LS-MIMO channels, the interaction of those messages will be captured through the mutual information functions. Taking into account the interaction of the LS-MIMO signal detection and the protograph LDPC decoding into the design is what differentiates our design framework from the previous ones where the single-layer graph is employed. Furthermore, as the reliability levels of the information bit from the observation nodes and the check nodes are improved after each iteration, the soft estimate, $\hat{x}[n, m]$, is thus improved after each iteration as well. Consequently, more amount of inter-stream interference in (3) will be canceled from the signal of interest after each iteration.

The LLR of the m^{th} transmitted symbol at the n^{th} receive antenna is given by

$$\begin{aligned}\alpha[n, m] &= \ln \frac{\Pr(\hat{y}[n, m]|\mathbf{H}, x[m] = +1)}{\Pr(\hat{y}[n, m]|\mathbf{H}, x[m] = -1)} \\ &= \frac{4\Re(h^*[n, m]\hat{y}[n, m])}{\Psi[n, m]},\end{aligned} \tag{5}$$

where

$$\Psi[n, m] = \sum_{k=1, k \neq m}^{M} |h[n, k]|^2(1 - |\hat{x}[n, k]|^2) + N_0. \tag{6}$$

The message $\alpha[n, m]$ is then passed to the variable node on the double-layer Tanner graph for the joint iterative detection and decoding receiver in [32], as shown in Fig. 2. The first layer is the bipartite graph from the observation nodes $\mathbf{y}$

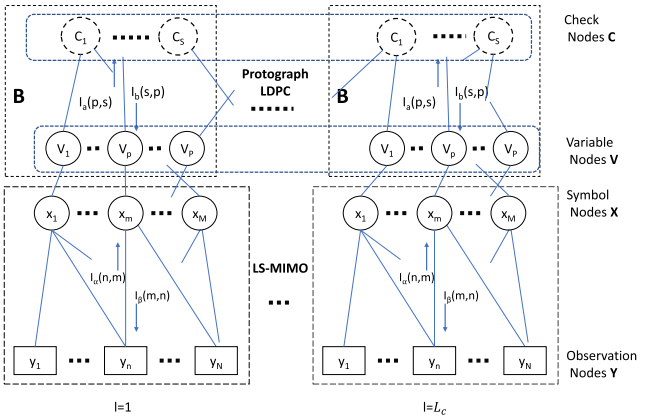

FIGURE 2. Double-layer graph for joint LS-MIMO signal detection and protograph LDPC decoding.

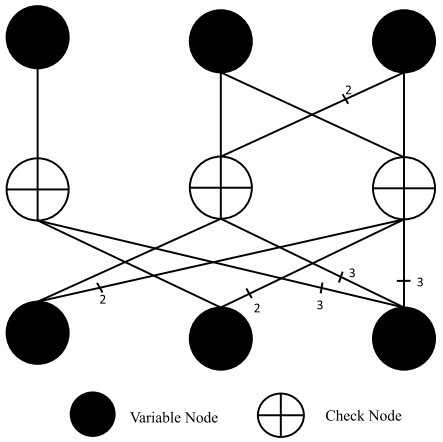

FIGURE 3. Protograph of the proposed protograph LDPC code in (20).

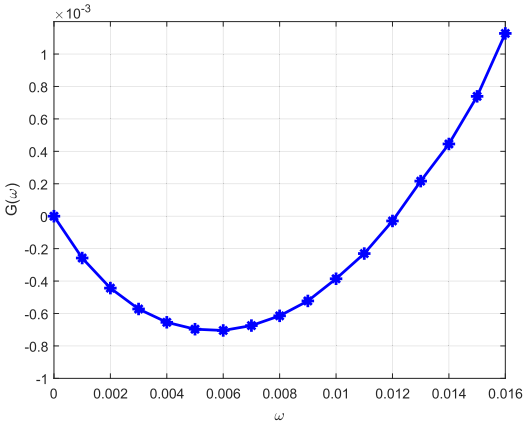

FIGURE 4. Weight spectral shape of the proposed protograph LDPC code in (20).

connecting to the symbol nodes **x**. The other layer is the protograph LDPC graph structure connecting the variable nodes **v** to the check node **c**. There is a one-to-one mapping between symbol nodes **x** and variable node **v**. Readers are referred to [8] on how to build the protograph LDPC from a protomatrix **B**.

With regard to how the joint LS-MIMO detection and protograph LDPC decoding graph impacts on the interference cancellation process, the expression (6) feeds us with a clear explanation. As analyzed above, the estimation of $x[m]$ at the n^{th} receive antenna becomes more and more accurate after each iteration. Because of that, the value of $|\hat{x}[n,m]|^2$ is closer to 1. This behavior means that the interference power (i.e., the first term in (6)) approaches zero. In short, the interference will be effectively canceled by incorporating the dynamic interaction of the messages on the double-layer graph into the design. Ultimately, the reliability levels of the posterior messages increases and the information bits are restored with a low error probability in comparison with the single-layer graph where the reliability levels at the output of the LS-MIMO detector is unchanged/static.

III. LS-MIMO-PEXIT ALGORITHM

To design a new protograph LDPC code for a $M \times N$ LS-MIMO system, one needs an analytical tool to evaluate, then find the optimal protomatrix **B** of the underlying protograph with S check nodes and P variable nodes (i.e., **B** has S rows and P columns). In this section, we introduce such an analytic tool that takes into account the features of the joint detection and decoding algorithm in Section II, as well as the propagation characteristics of LS-MIMO channels through the graph of joint LS-MIMO detection and protograph LDPC decoding, referred to as the LS-MIMO-PEXIT algorithm. The idea behind the LS-MIMO-PEXIT algorithm is to analyze the mutual information functions of messages passed through the double-layer graph, as shown in Fig. 2. It becomes obvious later that the LS-MIMO-PEXIT algorithm can be used as a good tool to judge if one protograph LDPC code outperforms another by evaluating their iterative decoding thresholds.

Adopting four types of mutual information in [30] as shown in Fig. 2, let $I_\alpha[n,m]$ denote the extrinsic mutual information between the LLR value sent by the n^{th} observation node to the m^{th} variable node and the m^{th} corresponding coded bit. $I_a[p,s]$ denotes the extrinsic mutual information between the LLR value sent by the p^{th} variable node to the s^{th} check node and the p^{th} corresponding coded bit. $I_b[s,p]$ is the extrinsic mutual information between the LLR value sent by the s^{th} check node to the p^{th} variable node and the p^{th} corresponding coded bit. $I_\beta[m,n]$ is the extrinsic mutual information between the LLR value sent by the m^{th} variable node to the n^{th} observation node and the m^{th} corresponding coded bit. To calculate those mutual informations, we use function $J(.)$ and $J^{-1}(.)$, which are given in [30].

The LS-MIMO-PEXIT algorithm is proposed as follows.

Step 0 Start with a signal-to noise ratio $(\frac{E_b}{N_0})_t$ and $I_\beta = 0$.

Step 1 Generate Q channel realizations of $\mathbf{H}$: $\mathbf{H}_q, q = 1, 2, \cdots, Q$. Calculate $\sigma_\beta = J^{-1}(I_\beta)$ [30].

Generate $\beta[m,n] \sim \mathcal{N}(\frac{\sigma_\beta^2}{2}, \sigma_\beta^2), \forall m = 1, \cdots, M$, $\forall n = 1, \cdots, N$. Using $\beta[m,n]$, the soft symbol estimation $\hat{x}[n,m]$ is calculated using the equation (4).

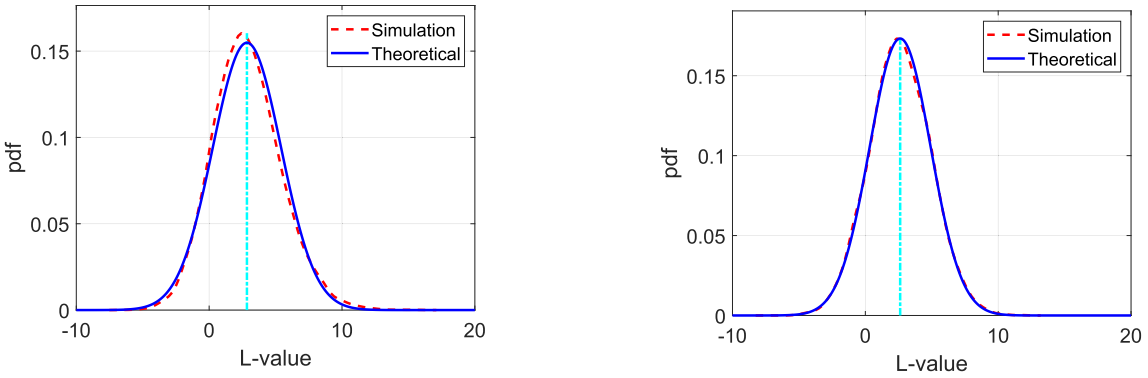

(a) 10×10 (b) 100×100

FIGURE 5. Probability density function of LLR messages: AR3A Code [13], coding rate $R = 1/2$.

Step 2 For a given channel realization $\mathbf{H}_q$, $q = 1, 2, \cdots, Q$, calculate $I_{\alpha,q}[n, m]$:

$$I_{\alpha,q}[n, m] = J(\sigma_{\alpha[n,m],q}), \tag{7}$$

where $\sigma_{\alpha[n,m],q} = \sqrt{\frac{|h_q[n,m]|^2}{\Psi_q[n,m]}}$ ($\Psi_q[n, m]$ is from (6)), and $J(x)$ is calculated using the expression in [30]. $I_\alpha[n, m]$ is the average of all channel realization: $I_\alpha[n, m] = \frac{1}{Q}\sum_{q=1}^{Q} I_{\alpha,q}[n, m]$.

Step 3 Calculate $I_a[p, s]$

$$I_a[p, s] = J\left(\sqrt{\sigma^2_{\alpha[p]} + \sigma^2_{b[p]}}\right), \tag{8}$$

where $\sigma^2_{b[p]} = \sum_{r\in N_c(p)\setminus s} \mathbf{B}[r, p][J^{-1}(I_b[r, p])]^2$, $\sigma^2_{\alpha[p]} = \sum_{n\in N_o(p)}[J^{-1}(I_\alpha[n, p])]^2$ in which $N_c(p)$ is the set of check nodes connected to the p^{th} variable node; $N_o(p)$ is the set of observation nodes connected to the p^{th} variable node; and $\mathbf{B}[r, p]$ is the $[r, p]$ element of protomatrix $\mathbf{B}$.

Step 4 Calculate $I_b[s, p]$

$$I_b[s, p] = J\left(\sqrt{\sum_{r\in N_v(s)\setminus p} \mathbf{B}[s, r][J^{-1}(1 - I_{a[r,s]})]^2}\right). \tag{9}$$

where $N_v(s)$ is the set of variable nodes connected to the s^{th} check node.

Step 5 Calculate $I_\beta[m, n]$

$$I_\beta[m, n] = J\left(\sqrt{\sigma^2_{\alpha[m]} + \sigma^2_{b[m]}}\right), \tag{10}$$

where $\sigma^2_{b[m]} = \sum_{r\in N_c(m)} \mathbf{B}[r, m][J^{-1}(I_b[r, m])]^2$ and $\sigma^2_{\alpha[m]} = \sum_{r\in N_o(m)\setminus n}[J^{-1}(I_\alpha[n, m])]^2$.

Step 6 Calculate the sum of mutual information from two layers collected at the p^{th} variable node $I_{APP}[p]$:

$$I_{APP}[p] = J\left(\sqrt{\sigma^2_{\alpha[p]} + \sigma^2_{b[p]}}\right), \tag{11}$$

where $\sigma^2_{b[p]} = \sum_{r\in N_c(p)} \mathbf{B}[r, p][J^{-1}(I_b[r, p])]^2$ and $\sigma^2_{\alpha[p]} = \sum_{r\in N_o(p)}[J^{-1}(I_\alpha[r, p])]^2$.

Step 7 Repeate steps 1-6 to a maximum number of iteration, $\text{Iter}_{\max}$ or until $I_{APP}[p] = 1, \forall p = 1, 2, \cdots, P$. The iterative decoding threshold is the minimum $(\frac{E_b}{N_0})_t$ such that $I_{APP}[p] = 1, \forall p = 1, 2, \cdots, P$, for a given maximum number of decoding iterations.

The above LS-MIMO-PEXIT algorithm will be utilized to calculate the iterative decoding threshold, $\eta(\mathbf{B}, M, N, \text{Iter}_{\max})$, in the protomatrix optimization problem in the following section. Note that the lower the iterative decoding threshold, the better code performance since the iterative decoding threshold is defined as the minimum channel quality that supports the reliable iterative decoding of asymptotically large LDPC codes built from the corresponding protomatrix with a given maximum number of decoding iterations over the joint graph.

Remark 1: The proposed PEXIT algorithm for LS-MIMO channels differs from the conventional one in all steps, except Step 4. Distinctly, the features of the message-passing joint detection and decoding and LS-MIMO channels are taken into account to calculate the mutual information functions.

Remark 2: The parameter $\sigma^2_{a[p]}$ in (8) plays the role of σ^2_{ch}, the variance of the channel LLR messages, in the conventional PEXIT algorithm. As a result, one of the essential assumptions in the development of the PEXIT algorithm is that the channel LLR messages follow the symmetric Gaussian distribution. We verify the Gaussian assumption via Monte Carlo simulations and the probability density functions (pdf) of the channel LLR messages are plotted in Fig. 5. The discrepancy occurs in the case of the 10×10 MIMO configuration. However, the difference between the two happens in the small area around the mean of the L-value. In the tail areas, the theoretical and the simulation curves are tight together. In the case of the 100×100 LS-MIMO configuration, there is no distinction between the theoretical and simulation curves. In short, the assumption of Gaussian distribution is reasonable for both 10×10 and 100×100 MIMO configurations (See Fig. 5a and Fig. 5b).

Remark 3: Even though, $\sigma^2_{a[p]}$ in (8) plays the role of σ^2_{ch} in the conventional PEXIT algorithm, the value of $\sigma^2_{a[p]}$ will be changed from one iteration to another. Consequently, the extrinsic information from the LDPC decoding graph

helps to improve the extrinsic information of the MIMO detection graph thanks to the joint graph structure, and vice versa. In contrast, that quantity remains unchanged in the conventional PEXIT algorithm.

Remark 4: In this proposed LS-MIMO-PEXIT algorithm, the mutual function $I_\alpha[n, m]$ is treated differently for different (n, m) pairs, which are edges on the LS-MIMO part of the double-layer graph. The reason is that the mutual function $I_\alpha[n, m]$ receives different pieces of mutual information from incoming edges, each with different channel gains in the fading environment. These are the unique features of the proposed LS-MIMO-PEXIT algorithm.

Remark 5: Regarding to the selection of initial value of E_b/N_0 in Step 0, one can use the technique proposed in [13] by selecting the initial value of E_b/N_0, which is sufficiently small. The value of E_b/N_0 is then increased by an amount of 0.001 dB after each iteration. In contrast, we use the binary search algorithm, with respect to the E_b/N_0 variable, to obtain the iterative decoding threshold. We first choose a feasible range $[(E_b/N_0)_{min}, (E_b/N_0)_{max}]$ for the E_b/N_0, then the initial value of E_b/N_0 is initially set to the middle point of the feasible range. In this particular work, we choose the E_b/N_0 range of $[-8$ dB, 8 dB$]$. Consequently, the initial value of E_b/N_0 is 0 dB. In our experiments, the search algorithm is always converged with respect to the E_b/N_0 variable. As a result, the selection of the initial value of E_b/N_0 does not affect the performance of optimized LDPC codes.

IV. DESIGN PROTOGRAPH LDPC CODES

The protograph LDPC code design involves the search for a protomatrix $\mathbf{B}$ that has the lowest iterative decoding threshold while maintaining the linear minimum distance growth property. The protograph LDPC code design can thus be mathematically formulated as an optimization problem as follows:

$$\begin{aligned} &\min_{\mathbf{B}\in\mathcal{B}_{Z^+}} \ \eta(\mathbf{B}, N, M, \mathrm{Iter}_{\max}) \\ &\text{s.t.} \quad f_c(\mathbf{B}) \le 0 \text{ for } c = 1, 2, \cdots, C, \end{aligned} \tag{12}$$

where $\mathcal{B}_{Z^+}$ denotes a set of all matrices with non-negative entries. The output of cost function, $\eta(\mathbf{B}, M, N, \mathrm{Iter}_{\max})$, is the iterative decoding threshold value. Furthermore, the cost function is obtained by applying the LS-MIMO-PEXIT algorithm in Section III. $f_c(\mathbf{B}) \le 0, c = 1, 2, \cdots, C$ represent the set of constraints according the design guidelines of protograph LPDC codes [8].

Notice that there are three main dimensions involved in the optimization problem: 1) protomatrix $\mathbf{B}$ represents the code structure of a given coding rate; 2) a pair of M and N represents the LS-MIMO configuration; 3) $\mathrm{Iter}_{\max}$ represents the maximum number of decoding iterations which is often limited due to the latency constraint of a given wireless communication system.

Unlike existing protograph code designs, e.g., [7], [8], in the optimization problem (12) above, we take $\mathrm{Iter}_{\max}$ as a design parameter to optimize the protograph LDPC code for delay-limited applications. For that, we focus on the low-iteration regime (i.e., $\mathrm{Iter}_{\max} \le 50$ which is typical constraint in the literature [9]). Moreover, under such a strict limitation on the maximum number of decoding iterations, protograph LDPC codes with the non-punctured protograph structure used in this work are preferable to the ones with punctured nodes [10], [11]. This is because the punctured codes need a high number of decoding iterations to be useful and converged. As shown in the experiment section below, the non-punctured codes, including the proposed code and the code in [10], outperform the state-of-the-art punctured protograph LDPC codes such as AR3A codes [13] and standard 5G LDPC code [9]. Furthermore, in the scenarios where the number of decoding iterations is not limited, one can straightforwardly apply the proposed framework to design punctured protograph LDPC codes.

In addition, the cost function in (12) includes the LS-MIMO configuration via the parameters M and N to capture the behavior of the LS-MIMO detection graph. Since the graph of the LS-MIMO detection part is fully connected by the nature of the radio signal propagation, its protomatrix is an all-one matrix (i.e., all entries have value 1), and thus we omit the protomatrix for the LS-MIMO graph in the cost function. Nevertheless, the dynamic interaction between messages of the LS-MIMO detection graph and the messages of the protograph LDPC decoding graph is still captured in the cost function via the mutual information functions in Step 3, Step 5, and Step 6 of the LS-MIMO-PEXIT algorithm above. This in-depth observation explains and justifies the additional coding gain of the new protograph LDPC code compared to the state-of-the-art LDPC codes, as shown in Fig. 1 of Section I-A.

Using guidelines on the properties of a good protomatrix [8], we can narrow down the search space of the above optimization problem, allowing us to run the brute-force search with reasonable complexity. Specifically, we impose constraints on the structure of the protomatrix $\mathbf{B}$, having 3 rows and 6 columns (a non-punctured protograph with 6 variable and 3 check nodes), resulting in a coding rate of 1/2 as follows.

$$\mathbf{B}_{1/2} = \begin{pmatrix} e_{1,1} & e_{1,2} & e_{1,3} & e_{1,4} & 0 & 1 \\ e_{2,1} & e_{2,2} & e_{2,3} & e_{2,4} & 1 & 0 \\ e_{3,1} & e_{3,2} & e_{3,3} & e_{3,4} & 1 & 0 \end{pmatrix}_{3\times 6}, \tag{13}$$

where element $e_{s,p}$ in $\mathbf{B}_{1/2}$ is the number of parallel edges connecting the p^{th} variable node and the s^{th} check node in the LDPC decoding part of the joint protograph. The last two columns are pre-selected according to the design guideline on the number of degree-one variable nodes and degree-2 variable nodes [8].

The remaining four columns have a total of 12 unknown variables, $e_{s,p}, s = 1, 2, 3, p = 1, \cdots, 4$, to optimize. Their values determine the final protograph. Those variables are selected from the set $\{0, 1, 2, 3\}$. In other words, the maximum number of allowed parallel edges is 3. The corresponding constraints of the optimization problem in (12) for the

above matrix $\mathbf{B}_{1/2}$ are as follows [8]:

$$\begin{cases} f_1(\mathbf{B}_{1/2}): -e_{s,p} \leq 0, \ \forall s=1,2,3, p=1,\cdots,4 \\ f_2(\mathbf{B}_{1/2}): e_{s,p}-3 \leq 0, \ \forall s=1,2,3, p=1,\cdots,4 \\ f_3(\mathbf{B}_{1/2}): 3-(e_{1,1}+e_{2,1}+e_{3,1}) \leq 0 \\ f_4(\mathbf{B}_{1/2}): 3-(e_{1,2}+e_{2,2}+e_{3,2}) \leq 0 \\ f_5(\mathbf{B}_{1/2}): 3-(e_{1,3}+e_{2,3}+e_{3,3}) \leq 0 \\ f_6(\mathbf{B}_{1/2}): 2-(e_{1,4}+e_{2,4}+e_{3,4}) \leq 0. \end{cases} \tag{14}$$

The constraints $f_3(\mathbf{B}_{1/2}), f_4(\mathbf{B}_{1/2}), f_5(\mathbf{B}_{1/2})$ are imposed to guarantee the linear minimum distance growth, and the constraint $f_6(\mathbf{B}_{1/2})$ comes from the fact that a good protograph LPDC code can have up to the number of check nodes minus 1 or $(3-1=2)$ degree-2 variable nodes allowed in the final protograph [33]. It is noted that the constraint on the number of degree-2 variable nodes in the protomatrix is the necessary, but not the sufficient condition for a good LDPC code. However, imposing this constraint to narrow down the search space is a good practice for AWGN channels in the literature, [7], [8]. We performed an experiment for LS-MIMO channels by searching for a best protomatrix on the full search space (i.e., we impose only two constraints $f_1(\mathbf{B}_{1/2}): -e_{s,p} \leq 0$ and $f_2(\mathbf{B}_{1/2}): e_{s,p}-2 \leq 0$). The experiment result reveals that the best protomatrix follows the guideline above. That is, the best protomatrix has a maximum of two degree-2 variables, one degree-1 variable, and all remaining variables have degrees higher than 3. Therefore, we employ the guideline to design new protograph LDPC codes for LS-MIMO channels in this paper.

To design new protograph LDPC codes that have higher coding rates, for example $2/3, 3/4, 4/5$, the lengthening technique, [7], [8], is employed so that the search space is feasible even when the size of protomatrix increases. Specifically, the structure of the protomatrix for high coding rates, $R=\frac{n+1}{n+2}, \forall n=1,2,\ldots$, are given by

$$\mathbf{B}_{n+1/n+2} = \left(\begin{array}{ccc|c} e_{1,1} & e_{1,2} & e_{1,3} & \\ e_{2,1} & e_{2,2} & e_{2,3} & \mathbf{B}_{n/n+1} \\ e_{3,1} & e_{3,2} & e_{3,3} & \end{array}\right)_{3\times(6+3n)}, \tag{15}$$

and their corresponding constraints for the optimization problem in (12) are written as

$$\begin{cases} f_1(\mathbf{B}_{n+1/n+2}): -e_{s,p} \leq 0, \quad \forall s,p=1,2,3 \\ f_2(\mathbf{B}_{n+1/n+2}): e_{s,p}-3 \leq 0, \quad \forall s,p=1,2,3 \\ f_3(\mathbf{B}_{n+1/n+2}): 3-(e_{1,1}+e_{2,1}+e_{3,1}) \leq 0 \\ f_4(\mathbf{B}_{n+1/n+2}): 3-(e_{1,2}+e_{2,2}+e_{3,2}) \leq 0 \\ f_5(\mathbf{B}_{n+1/n+2}): \tau-(e_{1,3}+e_{2,3}+e_{3,3}) \leq 0 \end{cases} \tag{16}$$

The parameter τ in the constraint $f_5(\mathbf{B}_{n+1/n+2})$ is equal 2 if the number of degree-2 variable nodes in $\mathbf{B}_{n/n+1}$ is 1, and it is equal 3 if the number of degree-2 variable nodes in $\mathbf{B}_{n/n+1}$ is 2. Again, the value of τ is selected according to the guideline above to guarantee that the maximum number of degree-2 variables is 2 as suggested by [33]. Using structural protomatrices in (15) results in a coarse resolution of the coding rate (i.e., $1/2, 2/3, 3/4$,..). However, one can employ the LS-MIMO-PEXIT algorithm in Section III and design approach proposed in [8] to obtain granular resolution of the coding rate.

V. EXPERIMENT RESULTS AND DISCUSSIONS

We carry out the code search with $\text{Iter}_{\max}=20$ and $\text{Iter}_{\max}=50$ and $M=10, N=10$ (i.e., 10×10 LS-MIMO configuration). We are interested in a small number of decoding iterations because the low latency is one of the critical requirements in the future wireless communications [5], [6]. For example, Zhang *et al.* [5], specify the latency of 6G wireless networks that is in order of ten microseconds, which is 10 and 100 times shorter than the 5G and 4G wireless systems, respectively. The optimal protomatrices for the coding rate of $1/2, 2/3, 3/4$ are given below:

$$\mathbf{B}_{1/2}^{20iter.} = \begin{pmatrix} 3 & 1 & 1 & 0 & 0 & 1 \\ 2 & 1 & 2 & 2 & 1 & 0 \\ 3 & 2 & 0 & 1 & 1 & 0 \end{pmatrix}_{3\times 6}, \tag{17}$$

$$\mathbf{B}_{2/3}^{20iter.} = \left(\begin{array}{ccc|c} 3 & 0 & 0 & \\ 2 & 3 & 0 & \mathbf{B}_{1/2}^{20iter.} \\ 3 & 0 & 2 & \end{array}\right)_{3\times 9}, \tag{18}$$

$$\mathbf{B}_{3/4}^{20iter.} = \left(\begin{array}{ccc|c} 3 & 0 & 0 & \\ 2 & 2 & 2 & \mathbf{B}_{2/3}^{20iter.} \\ 1 & 1 & 1 & \end{array}\right)_{3\times 12}. \tag{19}$$

$$\mathbf{B}_{1/2}^{50iter.} = \begin{pmatrix} 3 & 1 & 0 & 0 & 0 & 1 \\ 3 & 0 & 1 & 2 & 1 & 0 \\ 3 & 2 & 2 & 1 & 1 & 0 \end{pmatrix}_{3\times 6}, \tag{20}$$

$$\mathbf{B}_{2/3}^{50iter.} = \left(\begin{array}{ccc|c} 3 & 0 & 0 & \\ 3 & 1 & 1 & \mathbf{B}_{1/2}^{50iter.} \\ 1 & 2 & 2 & \end{array}\right)_{3\times 9}, \tag{21}$$

$$\mathbf{B}_{3/4}^{50iter.} = \left(\begin{array}{ccc|c} 2 & 1 & 0 & \\ 2 & 0 & 0 & \mathbf{B}_{2/3}^{50iter.} \\ 1 & 2 & 3 & \end{array}\right)_{3\times 12}. \tag{22}$$

It should be noted that those protomatrices in (17) - (22) are not necessary to be the ones that have the lowest iterative decoding thresholds. Observing from our practical design experience that the protomatrix with the lowest iterative decoding threshold sometimes has the error-floor behavior. Fortunately, we observe from our code design experience that there exists the error-floor-free protomatrix from the set of 10 protomatrices with lowest iterative decoding thresholds. Incorporating the practical design experience, we introduce a two-step procedure to optimize the protograph LDPC codes as below:

- Step 1: The coarse step where we push a new protomatrix into a first-in-first-out (FIFO) buffer if its iterative decoding threshold, using the LS-MIMO-PEXIT algorithm, is lower than the one at the bottom input) of the FIFO buffer. Once a new protomatrix is pushed into the FIFO buffer, the protomatrix at the top of the FIFO buffer is pushed out. Consequently, when the coarse step finishes, we obtain a list of 10 protomatrices with

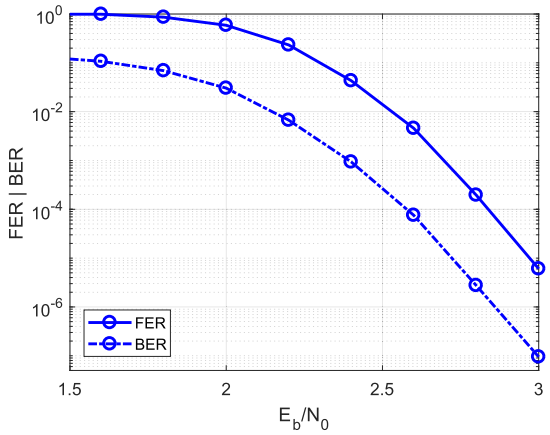

FIGURE 6. Illustration of the impact of the two-step procedure: protomatrix **B** in (17), coding rate $R = 1/2$, information blocklength 2400 bits, 20 iterations, 10 × 10 MIMO.

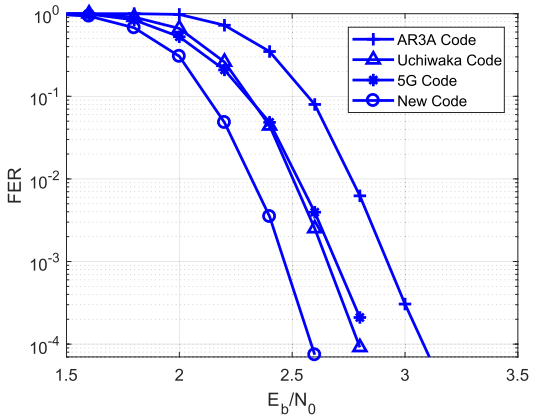

FIGURE 7. FER performance: coding rate $R = 1/2$, information blocklength 2400 bits, 20 iterations, 100 × 100 LS-MIMO.

the lowest iterative decoding thresholds sorted in the decreasing order.

- Step 2: The granular step where, from the top ten of protomatrices above, we perform intensive simulations to filter out the error-floor protomatrices. Finally, we choose the protomatrix that achieves FER = 10^{-5} at the lowest SNR from the error-floor-free list at the output of the filter.

To illustrate the advantage of the two-step design procedure mentioned above, both BER and FER performance of rate-1/2 protograph LDPC code in (17) are shown in Fig. 6. One can see that the reported protograph LDPC code does not have error-floor behavior at the FER = 10^{-5} or BER = 10^{-7}. This attribute of the proposed code makes it useful for the new generation of wireless networks where the ultra-reliability is often required.

Remark 6: It is worth noting that the two-step procedure is also useful when designing protograph LDPC codes for AWGN channels where the number of decoding iterations is limited, for example [11].

When designing new protograph LDPC codes, one is often interested in knowing how much the performance gap of the

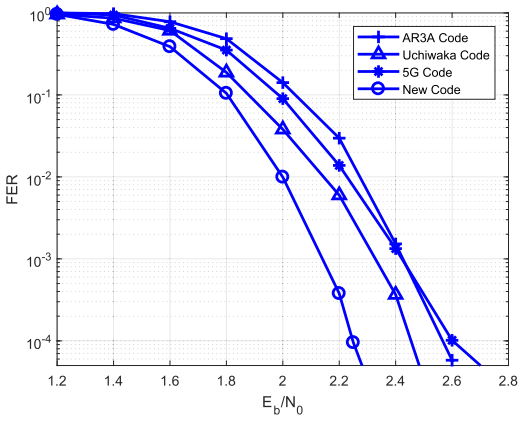

FIGURE 8. FER performance: coding rate $R = 1/2$, information blocklength 2400 bits, 50 iterations, 100 × 100 LS-MIMO.

new protograph LDPC codes to the theoretical benchmark (i.e., the capacity limit) is. To address this important question, we use the technique suggested in [34] to achieve the capacity limit for the 10 × 10 MIMO configuration via the Monte Carlo simulation. The resulting capacity limits, together with the iterative decoding thresholds for different targeted coding rates, are given in Table 1 for 20 iterations and Table 2 for 50 iterations, respectively.

We pick two protograph LDPC codes from the literature to compare with our new codes - AR3A codes [13] (punctured codes) and Uchiwaka codes [10] (non-punctured codes). The reason behind this selection is that the AR3A codes have three checks, same as the number of checks of our proposed codes. In addition, the AR3A codes were reported having the best performance in the fading environment [13]. Also, the Uchiwaka codes [10] are selected since they are the only codes, to our best knowledge, that satisfy two conditions: 1) belong non-punctured class; 2) were optimized for a small number of decoding iterations (20 iterations) even though this code family has four check nodes. Those two conditions are imposed to obtain a fair comparison with our proposed codes.

As shown in Table 1 and Table 2, our new protograph LDPC codes have the smallest gaps to the capacity limits at

TABLE 1. Gap to capacity (Eb/No dB), 10 × 10 MIMO channel, 20 iterations.

LS-MIMO	Rate	Cap. limit	Gap to capacity		
			New	Uchikawa	AR3A
10 × 10	$R = 1/2$	0.822	0.994	1.127	1.322
10 × 10	$R = 2/3$	1.842	0.728	0.825	0.919
10 × 10	$R = 3/4$	2.420	0.685	0.787	0.833

TABLE 2. Gap to capacity (Eb/No dB), 10 × 10 MIMO channel, 50 iterations.

LS-MIMO	Rate	Cap. limit	Gap to capacity		
			New	Uchikawa	AR3A
10 × 10	$R = 1/2$	0.822	0.580	0.686	0.703
10 × 10	$R = 2/3$	1.842	0.396	0.536	0.643
10 × 10	$R = 3/4$	2.420	0.404	0.537	0.605

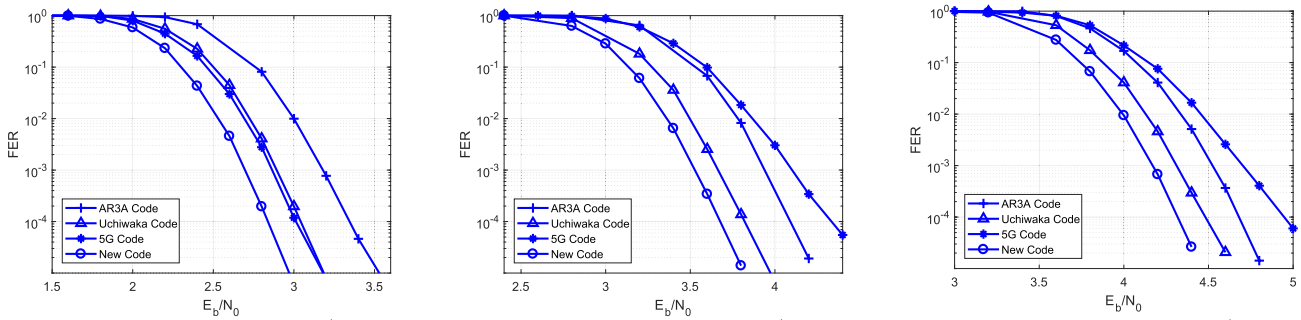

(a) Coding rate $R = 1/2$ (b) Coding rate $R = 2/3$ (c) Coding rate $R = 3/4$

FIGURE 9. FER performance: information blocklength 2400 bits, 20 iterations, 10 × 10 LS-MIMO.

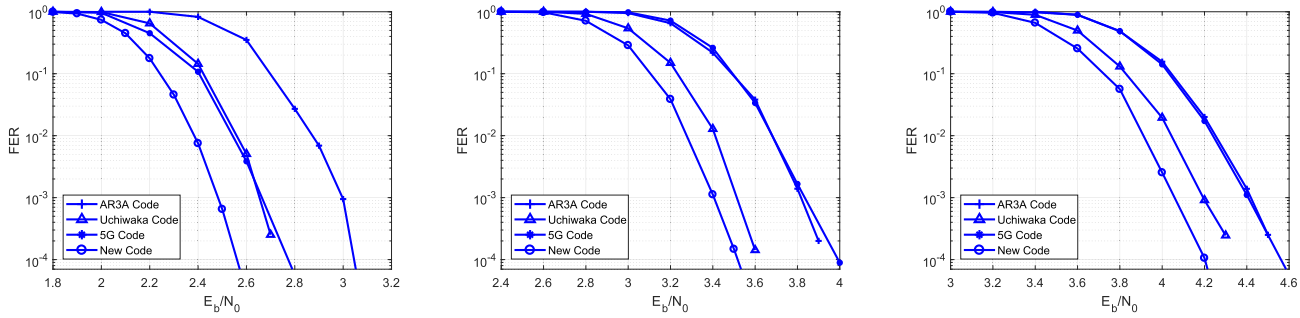

(a) Coding rate $R = 1/2$ (b) Coding rate $R = 2/3$ (c) Coding rate $R = 3/4$

FIGURE 10. FER performance: information blocklength 4800 bits, 20 iterations, 10 × 10 LS-MIMO.

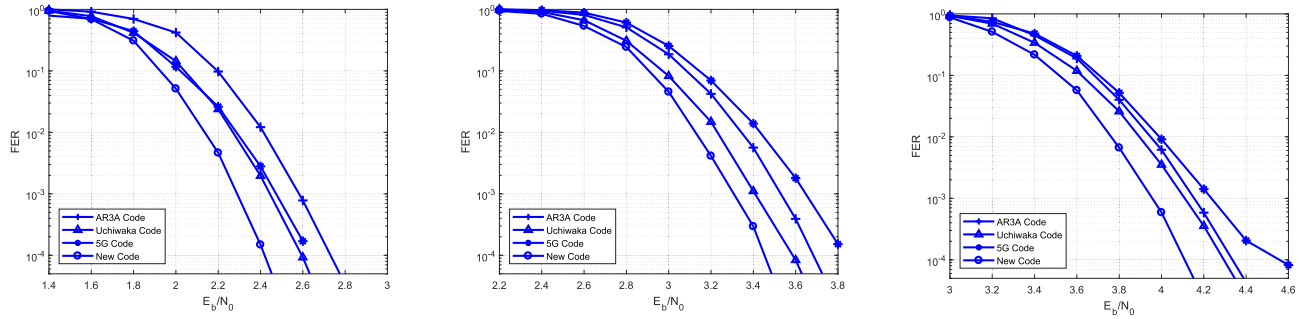

(a) Coding rate $R = 1/2$ (b) Coding rate $R = 2/3$ (c) Coding rate $R = 3/4$

FIGURE 11. FER performance: information blocklength 2400 bits, 50 iterations, 10 × 10 LS-MIMO.

all three coding rates and two constraints on the number of decoding iterations. Both the new codes and Uchiwaka codes outperform the AR3A codes since the number of decoding iterations is limited, and thus the non-punctured codes have better error-correcting capabilities. This observation was previously found for AWGN channels [10], [11], as well.

In more specific, we can see that the gaps to the capacity limits of the new protograph LDPC codes vary from 0.685 dB to 0.994 dB at $\text{Iter}_{\max} = 20$ iterations and from 0.404 dB to 0.58 dB at $\text{Iter}_{\max} = 50$ iterations, respectively. This means that by increasing the processing time to 2.5 times, we can potentially archive a coding gain from 0.3 dB at the coding rate of $1/2$ and 0.4 dB at the coding rate of $3/4$, approximately. We can achieve relatively the same coding gains via extensive simulations, as shown in Fig. 10 and Fig. 12 at FER $= 10^{-4}$. The good agreement between analytical results and simulation results proves that the LS-MIMO-PEXIT algorithm developed in Section III can be a useful tool not only to design new protograph LDPC codes but also to investigate the trade-off between the coding gain and the latency.

The next question is that whether the proposed protograph LDPC codes, which are optimized for the 10×10 MIMO configuration and their protomatrices are given in (17) - (22), outperform the state-of-the-art protograph LDPC codes in other LS-MIMO configurations or not. Employing the LS-MIMO-PEXIT algorithm in Section III, we can assess the iterative decoding thresholds of different selected code families under different LS-MIMO configurations. Table 3 and Table 4 present the iterative decoding thresholds of our

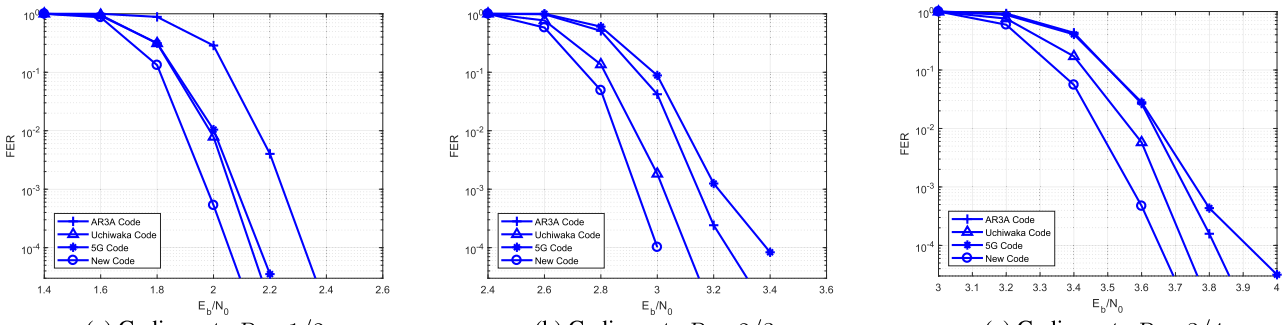

(a) Coding rate $R = 1/2$ (b) Coding rate $R = 2/3$ (c) Coding rate $R = 3/4$

FIGURE 12. FER performance: information blocklength 4800 bits, 50 iterations, 10 × 10 LS-MIMO.

TABLE 3. Performance prediction (decoding threshold (Eb/No, dB), 20 iterations) for various LS-MIMO configurations.

LS-MIMO	Rate	New	Uchikawa	AR3A
40×40	$R = 1/2$	1.705	1.832	1.992
40×40	$R = 2/3$	2.322	2.423	2.488
40×40	$R = 3/4$	2.783	2.877	2.908
40×100	$R = 1/2$	-2.511	-2.413	-2.109
40×100	$R = 2/3$	-1.959	-1.905	-1.704
40×100	$R = 3/4$	-1.499	-1.467	-1.313
100×100	$R = 1/2$	1.823	1.951	2.081
100×100	$R = 2/3$	2.364	2.466	2.512
100×100	$R = 3/4$	2.781	2.878	2.892

TABLE 4. Performance prediction (decoding threshold (Eb/No, dB), 50 iterations) for various LS-MIMO configurations.

LS-MIMO	Rate	New	Uchikawa	AR3A
40×40	$R = 1/2$	1.304	1.425	1.441
40×40	$R = 2/3$	2.00	2.142	2.146
40×40	$R = 3/4$	2.512	2.600	2.610
40×100	$R = 1/2$	-2.822	-2.859	-2.861
40×100	$R = 2/3$	-2.191	-2.218	-2.237
40×100	$R = 3/4$	-1.699	-1.745	-1.773
100×100	$R = 1/2$	1.427	1.566	1.586
100×100	$R = 2/3$	2.053	2.201	2.217
100×100	$R = 3/4$	2.519	2.601	2.611

proposed protograph LDPC codes and reference codes for 40×40, 40×100, and 100×100 LS-MIMO configurations. Based on the data given in Table 3 and Table 4, the proposed protograph LDPC codes also outperform the other code families in all LS-MIMO configurations and in both cases of iteration constraints (i.e., $\text{Iter}_{\max} = 20$ iterations and $\text{Iter}_{\max} = 50$ iterations). The simulation results, as shown in Fig. 7 and Fig. 8 for the 100×100 LS-MIMO configuration, verify the analytical results. In particular, the proposed protograph LDPC codes achieve a coding gain of 0.2 dB over the Uchikawa code and a coding gain of 0.4 dB over the AR3A code at FER $= 10^{-4}$ (almost the same as the coding gain of the 10×10 MIMO configuration). The observation from this investigation means that the performance of our porposed protograph LDPC codes is insensitive to the MIMO configuration.

To further highlight the advantages of our code design, we also compare our new codes with the 5G standard LDPC code [9] beside AR3A and Uchiwaka codes. As seen in Fig. 7 - Fig. 8 and Fig. 9 - Fig. 12, the new codes outperform all other codes [9], [10], [13] with a coding gain of 0.2 dB at FER $= 10^{-4}$ for the code rate of $1/2$. At the higher code rates, e.g., $2/3$ and $3/4$, the coding gains in comparison with the 5G LDPC code are about 0.4 dB and 0.5 dB, respectively.

As mentioned in Section IV, the constraint on the number of degree-2 variable nodes is only the necessary condition, not the sufficient condition for the minimum distance growth property. Nevertheless, this is good practice in the design of protograph LDPC codes for AWGN channels, [7], [8]. To investigate the usefulness of this constraint for LS-MIMO channels, we employ the method proposed in [35] to achieve the weight spectral shape and the typical minimum distance. Fig. 4 presents the weight spectral shape of the protomatrix in (20), whose protograph is shown in Fig. 3. One can see that the weight spectral function $G(\omega)$ crosses the horizontal axis at the value of $w^* = 0.012$. As a result, the typical minimum distance of the selected code is $0.012 \times n$, where n is the blocklength of a codeword. This verifies that the proposed protograph LDPC code in (20) possesses a minimum distance growth property. Accordingly, the design rule for AWGN channels is also practical/useful for LS-MIMO channels.

VI. CONCLUSION AND FUTURE WORKS

In this paper, we proposed the LS-MIMO-PEXIT algorithm, an analytical framework to not only evaluate the performance of off-the-shelf protograph LDPC codes but also to facilitate the design of new protograph LDPC codes under LS-MIMO channels. We demonstrated the usefulness of the tool by designing new protograph LDPC codes for LS-MIMO systems. The new protograph LDPC codes yield the coding gains varying from 0.2 dB to 0.4 dB over the off-the-shelf protograph LDPC codes. The coding gains are significant, especially for the high-speed wireless communications system where the data rate is up to Gbps and the power supply of the battery-operated devices is strictly limited.

Our investigation reveals that it strongly desires to further reduce the complexity of the proposed LS-MIMO-PEXIT

algorithm so that it is feasible to design the new protograph LDPC codes when the number of antennas becomes super-massive as proposed in 6G wireless networks. One possible approach, which is a very active research topic now, is to employ the machine learning techniques to unfold the iterations into network layers.

REFERENCES

[1] Y. Fang, G. Bi, Y. L. Guan, and F. C. M. Lau, "A survey on protograph LDPC codes and their applications," *IEEE Commun. Surveys Tutr.*, vol. 17, no. 4, pp. 1989–2016, 4th Quart., 2015.
[2] Y. Fang, G. Han, G. Cai, F. C. M. Lau, P. Chen, and Y. L. Guan, "Design guidelines of low-density parity-check codes for magnetic recording systems," *IEEE Commun. Surveys Tutr.*, vol. 20, no. 2, pp. 1574–1606, 2nd Quart., 2018.
[3] Y. Fang, P. Chen, G. Cai, F. C. M. Lau, S. C. Liew, and G. Han, "Outage-Limit-Approaching channel coding for future wireless communications: Root-protograph low-density parity-check codes," *IEEE Veh. Technol. Mag.*, vol. 14, no. 2, pp. 85–93, Jun. 2019.
[4] F. Steiner, G. Bocherer, and G. Liva, "Protograph-based LDPC code design for shaped bit-metric decoding," *IEEE J. Sel. Areas Commun.*, vol. 34, no. 2, pp. 397–407, Feb. 2016.
[5] Z. Zhang, Y. Xiao, Z. Ma, M. Xiao, Z. Ding, X. Lei, G. K. Karagiannidis, and P. Fan, "6G wireless networks: Vision, requirements, architecture, and key technologies," *IEEE Veh. Technol. Mag.*, vol. 14, no. 3, pp. 28–41, Sep. 2019.
[6] K. B. Letaief, W. Chen, Y. Shi, J. Zhang, and Y.-J.-A. Zhang, "The roadmap to 6G: AI empowered wireless networks," *IEEE Commun. Mag.*, vol. 57, no. 8, pp. 84–90, Aug. 2019.
[7] D. Divsalar, S. Dolinar, C. Jones, and K. Andrews, "Capacity-approaching protograph codes," *IEEE J. Sel. Areas Commun.*, vol. 27, no. 6, pp. 876–888, Aug. 2009.
[8] T. V. Nguyen, A. Nosratinia, and D. Divsalar, "The design of rate-compatible protograph LDPC codes," *IEEE Trans. Commun.*, vol. 60, no. 10, pp. 2841–2850, Oct. 2012.
[9] H. Li, B. Bai, X. Mu, J. Zhang, and H. Xu, "Algebra-assisted construction of quasi-cyclic LDPC codes for 5G new radio," *IEEE Access*, vol. 6, pp. 50229–50244, 2018.
[10] H. Uchikawa, "Design of non-precoded protograph-based LDPC codes," in *Proc. IEEE Int. Symp. Inf. Theory*, Jun. 2014, pp. 2779–2783.
[11] T. Van Nguyen and H. T. Nguyen, "The design of optimized fast decoding protograph LDPC codes," in *Proc. Int. Conf. Adv. Technol. for Commun. (ATC)*, Oct. 2016, pp. 282–286.
[12] G. Liva and M. Chiani, "Protograph LDPC codes design based on EXIT analysis," in *Proc. IEEE IEEE Global Telecommun. Conf. (GLOBECOM)*, Nov. 2007, pp. 3250–3254.
[13] Y. Fang, P. Chen, L. Wang, K.-K. Wong, and F. C. M. Lau, "Performance analysis of protograph-based low-density parity-check codes with spatial diversity," *IET Commun.*, vol. 6, no. 17, pp. 2941–2948, Nov. 2012.
[14] T. L. Narasimhan and A. Chockalingam, "EXIT chart based design of irregular LDPC codes for large-MIMO systems," *IEEE Commun. Lett.*, vol. 17, no. 1, pp. 115–118, Jan. 2013.
[15] D. C. Araújo, T. Maksymyuk, A. L. F. de Almeida, T. Maciel, J. C. M. Mota, and M. Jo, "Massive MIMO: Survey and future research topics," *IET Commun.*, vol. 10, no. 15, pp. 1938–1946, Oct. 2016.
[16] W. Fukuda, T. Abiko, T. Nishimura, T. Ohgane, Y. Ogawa, Y. Ohwatari, and Y. Kishiyama, "Low-complexity detection based on belief propagation in a massive MIMO system," in *Proc. IEEE 77th Veh. Technol. Conf. (VTC Spring)*, Jun. 2013, pp. 1–5.
[17] H. D. Vu, T. V. Nguyen, T. B. T. Do, and H. T. Nguyen, "Belief propagation detection for large-scale MIMO systems with low-resolution ADCs," in *Proc. Int. Conf. Adv. Technol. for Commun. (ATC)*, Oct. 2019, pp. 68–73.
[18] N. Samuel, T. Diskin, and A. Wiesel, "Learning to detect," *IEEE Trans. Signal Process.*, vol. 67, no. 10, pp. 2554–2564, May 2019.
[19] S. Takabe, M. Imanishi, T. Wadayama, R. Hayakawa, and K. Hayashi, "Trainable projected gradient detector for massive overloaded MIMO channels: Data-driven tuning approach," *IEEE Access*, vol. 7, pp. 93326–93338, 2019.
[20] E. Viterbo and J. Bouros, "A universal lattice code decoder for fading channels," *IEEE Trans. Inf. Theory*, vol. 45, no. 5, pp. 1639–1642, Jul. 1999.
[21] M. Mohammadkarimi, M. Mehrabi, M. Ardakani, and Y. Jing, "Deep learning-based sphere decoding," *IEEE Trans. Wireless Commun.*, vol. 18, no. 9, pp. 4368–4378, Sep. 2019.
[22] X. Jin and H.-N. Kim, "Parallel deep learning detection network in the MIMO channel," *IEEE Commun. Lett.*, vol. 24, no. 1, pp. 126–130, Jan. 2020.
[23] T. J. Richardson, M. A. Shokrollahi, and R. L. Urbanke, "Design of capacity-approaching irregular low-density parity-check codes," *IEEE Trans. Inf. Theory*, vol. 47, no. 2, pp. 619–637, Feb. 2001.
[24] Z. Li, L. Chen, L. Zeng, S. Lin, and W. Fong, "Efficient encoding of quasi-cyclic low-density parity-check codes," *IEEE Trans. Commun.*, vol. 53, no. 11, p. 1973, Nov. 2005.
[25] J. Thorpe, K. Andrews, and S. Dolinar, "Methodologies for designing LDPC codes using protographs and circulants," in *Proc. Int. Symp. Inf. Theory*, Jun./Jul. 2004, p. 238.
[26] C. Tang, M. Jiang, C. Zhao, and H. Shen, "Design of protograph-based LDPC codes with limited decoding complexity," *IEEE Commun. Lett.*, vol. 21, no. 12, pp. 2570–2573, Dec. 2017.
[27] Y. Fang, G. Zhang, G. Cai, F. C. M. Lau, P. Chen, and G. Han, "Root-Protograph-Based BICM-ID: A reliable and efficient transmission solution for block-fading channels," *IEEE Trans. Commun.*, vol. 67, no. 9, pp. 5921–5939, Sep. 2019.
[28] P. Chen, K. Cai, and S. Zheng, "Rate-adaptive protograph LDPC codes for Multi-Level-Cell NAND flash memory," *IEEE Commun. Lett.*, vol. 22, no. 6, pp. 1112–1115, Jun. 2018.
[29] Q. Chen, L. Wang, S. Hong, and Y. Chen, "Integrated design of JSCC scheme based on double protograph LDPC codes system," *IEEE Commun. Lett.*, vol. 23, no. 2, pp. 218–221, Feb. 2019.
[30] S. ten Brink, G. Kramer, and A. Ashikhmin, "Design of low-density parity-check codes for modulation and detection," *IEEE Trans. Commun.*, vol. 52, no. 4, pp. 670–678, Apr. 2004.
[31] T. V. Nguyen, H. D. Vu, D. N. Nguyen, and H. T. Nguyen, "Performance analysis of protograph LDPC codes over large-scale MIMO channels with low-resolution ADCs," *IEEE Access*, vol. 7, pp. 145145–145160, 2019.
[32] T. L. Narasimhan, A. Chockalingam, and B. S. Rajan, "Factor graph based joint Detection/Decoding for LDPC coded large-MIMO systems," in *Proc. IEEE 75th Veh. Technol. Conf. (VTC Spring)*, May 2012, pp. 1–5.
[33] S. Abu-Surra, D. Divsalar, and W. E. Ryan, "On the existence of typical minimum distance for protograph-based LDPC codes," in *Proc. Inf. Theory Appl. Workshop (ITA)*, Jan. 2010, pp. 1–7.
[34] B. M. Hochwald and S. ten Brink, "Achieving near-capacity on a multiple-antenna channel," *IEEE Trans. Commun.*, vol. 51, no. 3, pp. 389–399, Mar. 2003.
[35] E. Paolini and M. F. Flanagan, "Efficient and exact evaluation of the weight spectral shape and typical minimum distance of protograph LDPC codes," *IEEE Commun. Lett.*, vol. 20, no. 11, pp. 2141–2144, Nov. 2016.

HIEU D. VU received the B.Sc. degree in electronics and telecommunications from the Hanoi University of Science and Technology and the M.Sc. degree in digital communications from Kiel University. He is currently pursuing the Ph.D. degree in electrical engineering with the Posts and Telecommunications Institute of Technology (PTIT), Hanoi, Vietnam. His current research interests include source/channel coding and wireless MIMO communications with low-resolution ADCs.

THUY V. NGUYEN received the B.Sc. degree from the Hanoi University of Science and Technology (HUST), Hanoi, Vietnam, the M.Sc. degree from New Mexico State University, Las Cruces, NM, USA, and the Ph.D. degree from The University of Texas at Dallas, Richardson, TX, USA, all in electrical engineering. He was a member of Technical Staff with Flash Channel Architecture, Seagate, Fremont, CA, USA. He is currently a Lecturer with the Faculty of Information Technology, Posts and Telecommunications Institute of Technology (PTIT), Hanoi. His research interest includes coding theory and its applications in next generation communication systems.

DIEP N. NGUYEN received the M.E. degree in electrical and computer engineering from the University of California at San Diego (UCSD) and the Ph.D. degree in electrical and computer engineering from The University of Arizona (UA). He was a DECRA Research Fellow with Macquarie University, and a member of Technical Staff with Broadcom, CA, USA, and ARCON Corporation, Boston, consulting the Federal Administration of Aviation on turning detection of UAVs and aircraft and the US Air Force Research Laboratory on anti-jamming. He is currently a Faculty Member with the Faculty of Engineering and Information Technology, University of Technology Sydney (UTS). His current research interests include computer networking, wireless communications, and machine learning application, with emphasis on systems' performance and security/privacy. He has received several awards from LG Electronics, University of California at San Diego, The University of Arizona, the US National Science Foundation, and the Australian Research Council. He is an Associate Editor of the IEEE TRANSACTIONS ON MOBILE COMPUTING and a Guest Editor of IEEE ACCESS.

HIEU T. NGUYEN received the B.Sc. degree from the Hanoi University of Science and Technology, the M.Sc. degree from the University of Saskatchewan, Canada, and the Ph.D. degree from the Norwegian University of Science and Technology, all in electrical engineering. He is currently a Faculty Member with the Faculty of Technology, Natural Sciences, and Maritime Sciences, University of South-Eastern Norway (USN).